Int J Adv Manuf Technol (2014) 73:859–873
DOI 10.1007/s00170-014-5845-0

ORIGINAL ARTICLE

Optimal tolerance design for mechanical assembly considering thermal impact

G. Jayaprakash · M. Thilak · K. SivaKumar

Received: 9 November 2010 / Accepted: 7 April 2014 / Published online: 9 May 2014

Abstract In this paper, a cost–tolerance model based on neural network methods is proposed in order to provide product designers and process planners with an accurate basis for estimating the manufacturing cost. Tolerance allocation among the assembly components is carried out to ensure that the functionality and design quality are satisfied considering the effect of dimensional and geometric tolerance of various components of the assembly by developing a parametric computer aided design (CAD) model. In addition, deformations of various components of mechanical assembly due to inertia and temperature effects are determined and the same is integrated with tolerance design. The benefits of integrating the results of finite element simulation in the early stages of tolerance design are discussed. The proposed method is explained with an application example of motor assembly, where variations due to both dimensional and geometric tolerances are studied. The results show that the proposed methods are much effective, cost, and time saving than the ones considered in literature.

Keywords Tolerance allocation · Neural network · Inertia · Temperature effects · Finite element simulation · Deformation

Electronic supplementary material The online version of this article (doi:10.1007/s00170-014-5845-0) contains supplementary material, which is available to authorized users.

G. Jayaprakash (✉)
Department of Mechanical Engineering, Saranathan College of Engineering, Tiruchirappalli 620012, India
e-mail: jpjaya_74@yahoo.co.in

M. Thilak
Department of Mechanical Engineering, TRP Engineering College, Tiruchirappalli, India

K. SivaKumar
Department of Mechanical Engineering, Bannari Amman Institute of Technology, Sathyamangalam 638401, India

1 Introduction

The primary objective of tolerance design is to distribute assembly tolerances between components. Applications of tolerance design require mathematical modeling of cost–tolerance relationships. Distinct operations have different cost-tolerance relationships. Most researchers agree that there is an inverse relationship between tolerance and cost [1]. Numerous cost-tolerance functions for various machining operations, which include turning, milling, drilling, grinding, casting, etc., are given in the literature [2–5]. They include exponential, reciprocal squared, reciprocal power, reciprocal, discrete, polynomial, B-spline, and hybrid form, etc., functions. These functions are established by regression analysis using empirical data from the real manufacturing. Tolerance synthesis is more complicated in an assembly due to the fact that a manufacturing process for an assembly consists of placing various components and subassemblies jointly to establish a finished product with an expected functionality. Once the cost-tolerance relationships have been generated, mathematical models for tolerance synthesis can be built to obtain the optimal tolerance design. In real manufacturing environments, the cost–tolerance relationship exits. However, it is quite difficult to obtain the parameters of cost–tolerance functions. Using traditional methods of regression analysis, one must make assumptions about the form of the regression equation or its parameters, which may not be valid in practice. Regression analysis may be inclined to generate numerous tables of results. These results are frequently difficult for design engineers to interpret without a statistics background. In addition, the previously developed forms of cost–tolerance relationships may not be suitable for considering quality loss [6]. Quality loss is the cost incurred in a product life that occurs after the product is sold. The quality loss is also ideal function for establishing practical manufacturing tolerances.

Neural network approach though regarded as a statistical method, it is used to learn a feature hidden within the design experiment. Chen and Chan [7] presented a procedure that included a neural network and a fine tuning algorithm to optimize the tolerance allocations for achieving minimum cost. Kopardekar and Anand [8] presented a neural network based method for the tolerance allocation, which took the machinability and the machine tool inaccuracy into consideration. In addition, neural network can be constructed without any assumptions concerning the functional form of the relationship between predictors and responses [9]. Therefore, the neural network approach outperforms the conventional statistical modeling approach in terms of analyzing experimental data [10]. Mu-Chen chen et al. [11] used neural network to develop cost–tolerance function. Lin [12] developed cost–tolerance analysis model based on a neural network method. Yang [13] used neural network approach to optimize tolerance design to determine component tolerance of assemblies.

When designers are performing tolerance design, they generally assume that the parts for assembly are not geometrically perfect with regard to their nominal geometry. It is also assumed that they have no flexibility. The assumption that parts and therefore mechanisms are rigid forces us to solve hyper-statically, thereby increasing precision, as well as to add manufacturing constraints. Thus, the price will increase, in this case, an iso-static solution can be used, or clearance can be increased, which makes good geometrical defects. Today, part sizes are optimized as much as possible. Therefore, the sizes of parts are decreasing. Thus, the flexibility of parts increases. Moreover, the elastic displacements are not negligible or comparable to dimension tolerances of many parts. It is also observed that elastic displacements of parts and joints are of same nature. Therefore, it is necessary to build models where elastic displacements and joints are mixed with tolerancing.

In general, the component variation is recognized as a major problem in elastic assembly processes. A number of methods and tools have been developed to simulate the assembly processes and to analyze the assembly variation. Currently, the variation analysis of non-rigid assemblies has attracted many researchers. Liu and Hu [14] considered the compliant nature of sheet metal parts and proposed an influence coefficients method to analyze the effect of component variation and assembly spring-back on the assembly variation by applying linear mechanics and statics. The influence coefficients method was a key technique to get the component stiffness matrix. Camelio et al. [15] successfully extended this approach to model the product variation in multi-station assembly systems. Hu [16] set up the "stream of variation" theory for the automotive body assembly variation analysis. Ceglarek and Shi [17] proposed a new variation analysis methodology for the sheet metal assembly based on physical/functional modeling of the fabrication error using a beam-based model. Hu et al. [18] developed a numerical simulation method for the assembly process incorporating compliant non-ideal components. The effects of various variation sources were analyzed. In addition, Heieh and Oh [19] represented a procedure for simulating the combined effects of deformation and dimensional variation in the elastic assembly. Sampers and Giordano [20] considered elastic displacements in 3D tolerancing models, where they proposed four models and carried out synthesis of displacements by adding clearance displacements, distortion displacements and elastic displacements. Liao and Wang [21] proposed a novel method to investigate the influence of the component surface micro-geometry on the assembly dimensional variation by applying the finite element method and fractal geometry. Manarvi and Juster [22] used finite element simulation as a virtual tool for tolerance allocation in assembly design. Pierre et al. [23] has integrated thermo-mechanical strains into tolerance analysis, where he has used finite element method to determine the strains. The effect of inertia on tolerance design of mechanical assembly has been studied [24]. In addition to inertia, even the effect of temperature on tolerance design has been investigated [25].

An extensive review of previous works in applications of neural network and finite element simulation in tolerance design are presented. Major conclusions of this review are summarized as follows: (1) A couple of efforts in the literature addressed the usage of neural network to develop cost–tolerance function of tolerance design. However, neural network models have to be used in conjunction with intelligent optimization technique, which is absent in the literature; (2) Finite element simulation has been used by a few researchers in tolerance design to determine the effect of deformation of sheet metal parts in the assembly. However, usage of finite element simulation to consider the effect of deformation of all parts of the assembly due to inertia and change in operating temperature, is absent in the literature; (3) An integrated tolerance design approach, considering the effect of deformation of all parts of the assembly due to inertia and change in operating temperature, using finite element simulation and intelligent optimization technique is absent in the literature.

To overcome limitations of the existing works and advance the knowledge base of tolerance design, this work aims at establishing an integrated tolerance design approach to investigate the effect of deformation of all parts of the assembly using finite element simulation and intelligent optimization technique. By using finite element simulation, the dimensional variations of final assembly can be predicted during the design and process planning stage itself thereby minimizing its effect on final quality of the

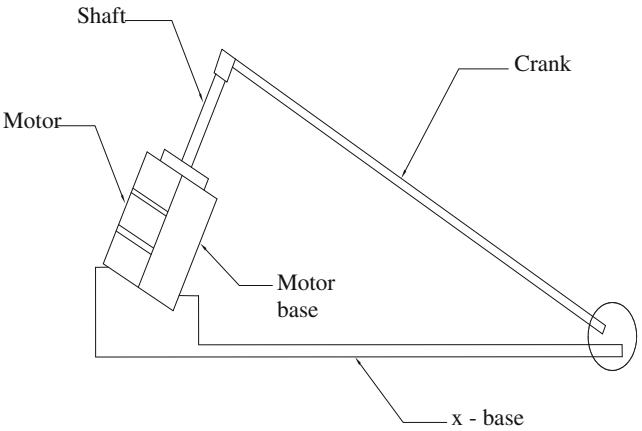

Fig. 1 Motor assembly

assembly. Intelligent optimization technique is used to optimize tolerance design process where the objective is to minimize total manufacturing cost. The deformation has been included in the functional constraint equation in order to ensure that the optimal tolerance values obtained as end product of optimization satisfies functional requirements.

The rest of this study is organized as follows: Section 2 deals with effect of temperature and gravity on parts of the mechanical assembly. Section 3 deals with modeling and simulation of the assembly components Section 4 presents the tolerance design problem formulation to obtain the optimal solutions. Section 5 presents results obtained by various approach and discussions on the same. The conclusions are given in Section 6.

2 Thermal impact and gravity effect

As temperature increases, size increases. This phenomenon is known as thermal expansion. The increase in length ΔL caused by the change in temperature ΔT is α L ΔT. α is the average coefficient of linear expansion for given material. Thermal expansion plays an important role in many applications. For example, thermal expansion joints must be installed in buildings, concrete highways, and bridges to compensate for change in dimensions owing to temperature variation. Power lines are hung slack to prevent the thermal shrinkages caused by cold weather from increasing the tension on the lines to breaking point. Generally, the amount of compensation or slack in the above example is calculated "roughly" to achieve the objectives because designing for thermal impact is not well understood technology, except for those who practice it on regular basis. There is a tendency to over design, just to be on the safe side. However, in situation in which a precise design compensation, slack, dimension or tolerance is required in order for the product to function properly, thermal impact must be taken into effect during the design process, particularly when a complicated product with multiple components and various materials

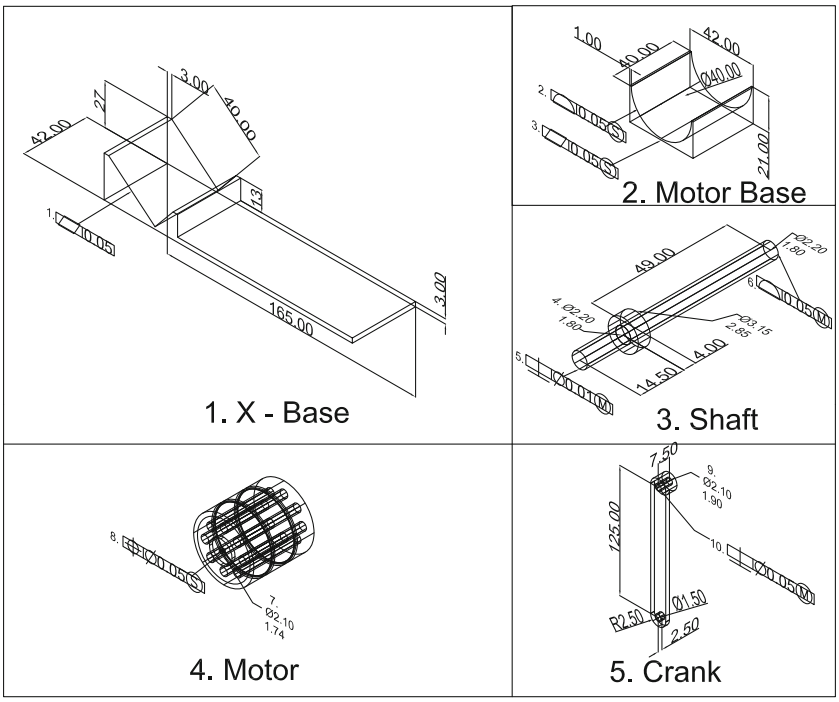

Fig. 2 Components of motor assembly

operates under a wide range of temperature. Thermal effect can be reduced either by thermal control, which provides cooling or heating devices as part of product to regulate the operating temperature or by selecting materials which have small coefficient of thermal expansion. In addition to thermal effect, gravity effect also results in deformation (change in length) of a component. Gravity effect like self weight, angular velocity produces significant amount of deformation on the component. The amount of deformation produced by the gravity effect is directly proportional to density of the material. In this work, the deformation due to thermal impact and gravity effect are determined using finite element analysis (FEA) and they are suitably incorporated in the tolerance stack up equation of tolerance design, thereby loosening tolerance requirement of critical components. Since the deformation is included in the early stages of design, the optimal tolerance values of some critical components of the assembly obtained are higher than that of those vales obtained by conventional method, resulting in reduction of the total manufacturing cost of the assembly.

3 Modeling and finite element simulation

This application is related to motor assembly (Fig. 1) which consists of an *x*-base, crank, shaft, and motor base. Figure 2 shows the graphical representation of the motor assembly with dimensioning and tolerancing schemes. Table 1 provides some relevant information regarding various components of the motor assembly. The ordering number in the first row of Table 1 is also given in the component drawings for the purpose of easy association. The objective is to allocate appropriate tolerance so that there is sufficient clearance between the crank and *x*-base, as shown in Fig. 1.

In order to determine the features which have an effect on clearance measurement, an abstracted feature parameter model was developed [26]. In this model, all the features potentially involved in the stack are initially abstracted to the very basic geometric entities. Then, these features are represented by corresponding parameters. Finally, a standard set of distance and angular relation between the simplified feature entities are used to build a constraint model. Since an assembly consists of many components connected together by various types of kinematic joints, the effect of the geometric feature tolerances associated with each of the joints may result in translational variation or rotational variation [27], which is usually smaller than the size tolerances on the same parts.

Table 2 [27] lists the rotational and translational variations associated with corresponding geometric feature

Table 1 Dimensioning and tolerancing schemes for motor assembly

Tolerance and size no.	1	2	3	4	5	6	7	8	9	10
Component	*x*-base	Motor base	Motor base	Motor shaft	Motor shaft	Motor shaft	Motor	Motor	Crank	Crank
Geometry Feature	Flatness	Profile	Flatness	Size	Perpendicularity	Profile	Size	Position	Size	Perpendicularity
Illustration	Surface on *x*-base	Surface on motor base	Surface on the bottom of motor base	Size of the shaft (with target value 2.0 cm)	Perpendicularity of shaft	Profile of shaft	Hole size of motor	Hole position of motor	Hole size of crank	Hole perpendicularity of crank
Possible tolerance levels	0.050	–	0.040	0.100	0.050	–	–	–	–	–
	0.075		0.060	0.150	0.075					
	0.100		0.080	0.200	0.1					
Influence on clearance?	Yes	No	Yes	Yes	Yes	No	No	No	No	No

Table 2 Rotational and translational variations associated with corresponding geometric feature tolerance-kinematic joint combinations in 2D [25]

GeomTol joints	▱	—	○	⌀	⌓	//	⊥	∠	↗↗	◎	⊕
Planar	R	R			R	R	R	R	RT	RT	
Cyl slider	T	T	T	T	T	T	T	T	T		
Edge slider	T	T	T	T	T	T	T	T	T	T	T
Revolute										T	T
Par cylind		T	T	T	T				T		

tolerance-kinematic joint combinations in 2-D. The extreme magnitude of tolerance variation dα for translational variation is given by Eq. 1 [27]. The extreme magnitude of tolerance variation dβ for rotational variation is given by Eq. 2 [27].

$$\mathrm{d}\alpha = \pm\frac{1}{2}(\mathrm{tol\,zone}) \tag{1}$$

$$\mathrm{d}\beta = \pm\tan^{-1}\left(\frac{\mathrm{tol\,zone}}{\mathrm{contact\,length}}\right) \tag{2}$$

In this motor assembly, the critical assembly feature is the clearance between the crank and *x*-base (Fig. 3). The assembly is of reasonable complexity, with about one dimensional variation and nine geometric variations as contributing sources. One of the geometric variations, x-base flatness is modeled as follows: The components *x*-base and motor base constitute a planar joint. From Table 2, the associated tolerance variation is found to be rotational variation. The extreme magnitude of tolerance variation dβ for the rotational variation is calculated as follows:

$$\mathrm{d}\beta = \pm\tan^{-1}\left(\frac{0.1}{40}\right) = 0.150^{\circ} \tag{3}$$

The *x*-base flatness is modeled as angle between two planes as shown in Fig. 4. Similarly, another geometric variation, the motor shaft perpendicularity is modeled as follows. The components motor shaft and motor constitutes cylinder slider joint. From Table 2, the associated tolerance variation is found to be translational variation. The extreme magnitude of

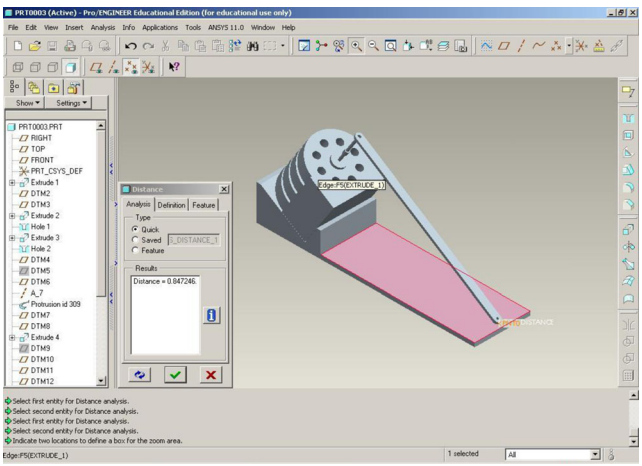

Fig. 3 Critical assembly feature—the clearance

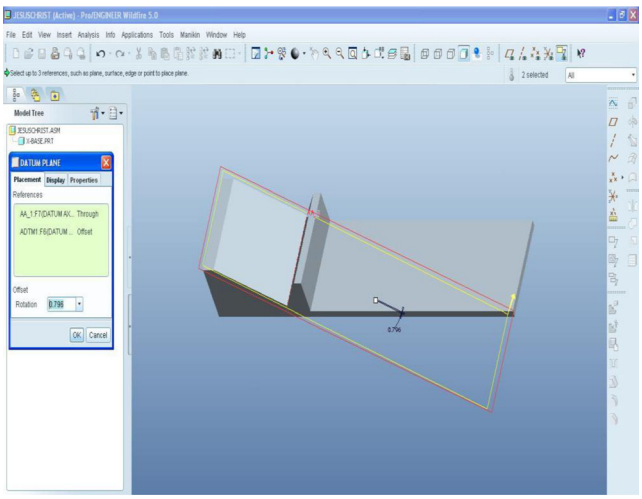

Fig. 4 x-base flatness feature

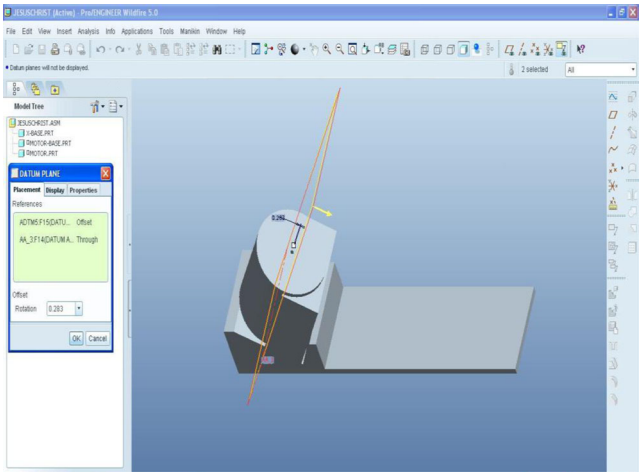

Fig. 5 Motor shaft perpendicularity feature

tolerance variation dα for the translational variation is calculated as follows:

$$d\alpha = \pm\frac{1}{2}(0.10) = \pm 0.050\,\text{cm} \tag{4}$$

The motor shaft perpendicularity is modeled as angle between two planes as shown in Fig. 5. Similarly, the remaining seven geometric variations have been modeled in addition to one dimensional variation. Once the model has been developed, the next step is to determine the contribution by each variation source towards variation of the critical assembly feature. It depends upon the sensitivity of the clearance to each component variation. Based on sensitivity analysis, *x*-base flatness, motor base flatness, motor shaft size and motor shaft perpendicularity are the features which have an effect on clearance measurement.

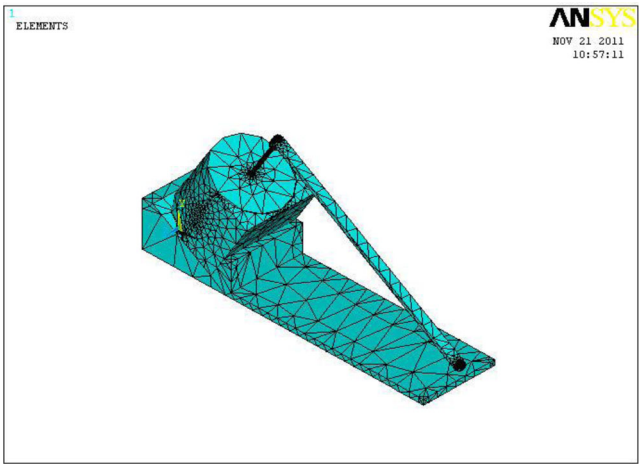

Fig. 6 Finite element model of the motor assembly

Once a three-dimensional model of the assembly is created, the next step is to develop a finite element model of the same to determine deformation of various components and their effects on the clearance. The assembly consists of five components and there are four contact pairs between them. Coupled field analysis has to be carried out to combine static and contact analysis together. The coupling is accomplished by direct coupling method using couple field elements suitable for both static and contact analysis. The elements used in the analysis are SOLID 92 and elements used to define the four contact pairs are CONTA173 and TARGE170. Contact occurs when the element surface penetrates one of the target segment elements on a specified target surface. The finite element model generated (Fig. 6) has 100,016 elements. Out of this 95,066 are SOLID 92, 2,298are CONTA173 and 2,652 TARGE170. Once a finite element model is generated, the next step is to determine deformation due to gravity and temperature effect. Material properties required for this analysis are modulus of elasticity, Poisson's ratio density and thermal coefficient of expansion. The material properties of various elements of the analysis are listed in Table 3. The next step is to define loads and constraints required for the analysis. The major constraints in the presented design are variation of thermal environment both within and among various application categories and inertia effects. Hence, the design which withstands temperature variation and inertia must be considered in the present case. If the temperature is 25 °C when the motor is assembled and then varies between 10 and 40 °C during application; if the self weight of the shaft is considered and inertia effect due to angular velocity of the shaft is considered, then the deformation is determined using FEA. In order to account for inertia effect like gravity appropriate values for g (9.81 m/s^2) is given. Then the deformation is calculated for three levels of temperature within the operating range (i.e., 10, 25 and 40 °C). In order to prevent rigid body motion, all degrees of freedom of

Table 3 Material properties of various components of the assembly

Sample no	Material property	*x*-base	Motor base	Motor	Shaft	Crank
1	Modulus of elasticity, E (N/mm^2)	1E05	1E05	1E05	2.060E05	2.060E05
2	Poisson's ratio (ν)	0.23	0.23	0.23	0.30	0.30
3	Density (kg/mm^3)	7200E−09	7200 E−09	7200 E−09	7840 E−09	7840 E−09
4	Coefficient of linear expansion per °C	9E−06	9E−06	9E−06	11.1E−06	11.1E−06

Table 4 Mass properties of components and assembly (Motor assembly)

Sample no	Mass property	*x*-base	Motor base	Motor	Shaft	Crank	Assembly
1	Volume in mm^3	5.204E+07	1.015E+07	5.017E+07	1.910E+05	1.330E+06	1.139E +08
2	Mass in kg	374.699	73.060	361.226	1.497	10.430	820.914
3	IXX about C.G in kg m^2	7.234E+06	1.147E+06	8.435E+06	6.764E+01	2.761E+03	3.207E +07
4	IYY about C.G in kg m^2	7.903E+07	2.899E+06	8.435E+06	5.690E+04	1.522E+05	9.802E+07
5	IZZ about C.G in kg m^2	7.524E+07	2.098E+06	7.238E+06	5.690E+04	1.523E+06	1.080E+08
6	Principal M.I-I1 in kg m^2	6.676E+06	1.147E+06	7.238E+06	6.747E+01	2.738E+03	3.031E+08
7	Principal M.I-I2 in kg m^2	7.524E+07	2.098E+01	8.435E+06	5.690e+04	1.522E+06	9.979E+07
8	Principal M.I-I3 in kg m^2	7.958E+07	2.899E+01	8.435E+06	5.690E+04	1.523E+06	1.08E+08
9	Radius of gyration—R1 in mm	133.479	125.312	141.555	6.711	16.200	1.921E+02
10	Radius of gyration—R2 in mm	448.099	169.442	152.814	194.913	381.974	3.487E+02
11	Radius of gyration—R3 in mm	460.842	199.184	152.814	194.913	382.172	3.627E+02

nodes defining the bottom surface of the *x*-base are constrained.

Once the loads and constraints are applied on the finite element model, the next step is to begin the solution phase. During the solution phase, the governing algebraic equations are assembled in matrix form and the unknown value of the primary field variable has been computed. The mass properties of all the components and the assembly have also been computed which are shown in Table 4. Among the mass properties, the mass of every component plays an important role while determining deformation due to inertia effect because the components undergo deformation due to self weight. In addition to mass, mass moment of inertia about centroid Ixx also affects the deformation. Figure 7 shows the deformation along *Y* direction (vertical direction) of various components of the assembly due to gravity effect. Figure 8 shows the variation of deformation along the length of the crank. The deformation is maximum at the free end as the crank is similar to cantilever beam fixed at the shaft end. Similarly, Fig. 9 shows the variation of induced von Mises stress along the length of the crank. The stress is maximum at the shaft end because in a cantilever beam stress will be maximum at support. The maximum value of deformation along *Y* direction (δg) is found to be −0.2525 cm and the maximum value of induced von Mises stress is found to be 1,883 N/cm^2. In order to determine the deformation along the *Y* direction due to effect of angular velocity, a subassembly model has been developed. The subassembly has the two rotating components of the main assembly. They are the crank and the motor shaft. Figure 10 shows the finite element model of crank and shaft subassembly. The finite element model generated (Fig. 10) has 42,157 elements. Out of this, 41,099 are SOLID 92, 398 are CONTA173 and 660 are TARGE170. In this analysis, the applied load is angular velocity which is determined as follows:

$$\overrightarrow{\omega} = \omega \times \overrightarrow{\lambda} \tag{5}$$

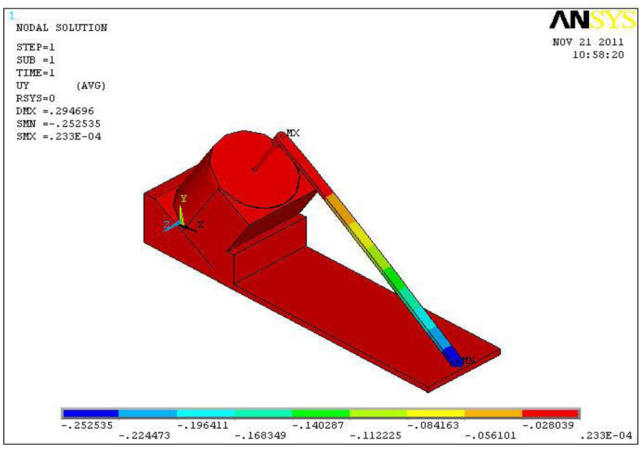

Fig. 7 Deformation along Y direction due to gravity effect

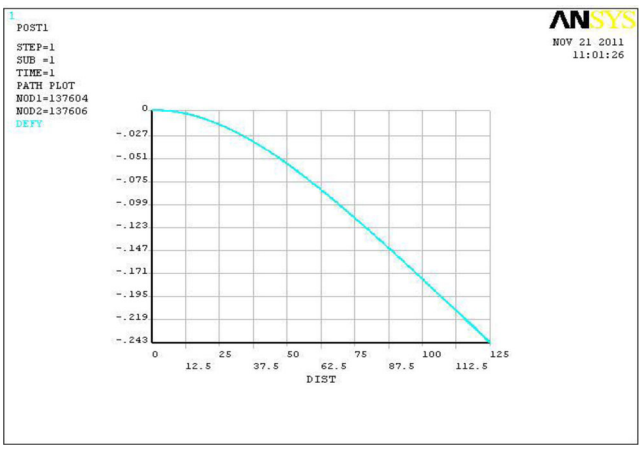

Fig. 8 Deformation-Y plot due to gravity effect

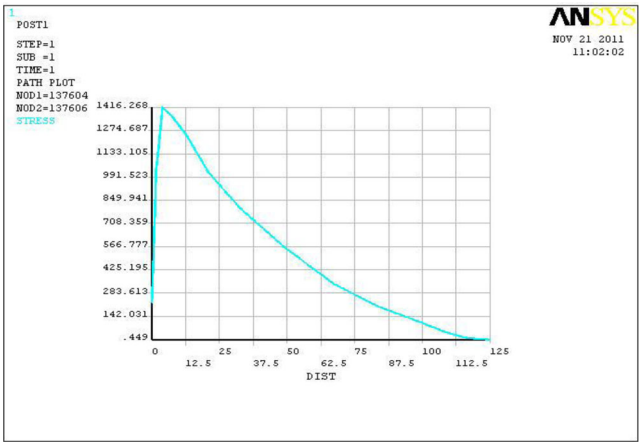

Fig. 9 von Mises stress plot due to gravity effect

$$\omega = \frac{2 \times \pi \times N}{60} \quad \text{rad/sec} \tag{6}$$

where N=100 rpm. The unit vector $\vec{\lambda}$ is calculated as follows.

$$\vec{\lambda} = \left\{ \frac{\left[(x_2 - x_1)\vec{i} + (Y_2 - Y_1)\vec{j} + (Z_2 - Z_1)\vec{k}\right]}{\left[(x_2 - x_1)^2 + (Y_2 - Y_1)^2 + (Z_2 - Z_1)^2\right]} \right\} \tag{7}$$

Once the loads and constraints are applied on the finite element model, the next step is to begin the solution phase. The mass properties of all the components of the assembly have also been computed which are shown in Table 5. Among the mass properties, the mass, mass moment of inertia and radius of gyration plays an important role while determining deformation due to angular velocity as the formula for centrifugal force=$m\omega^2 r$. Then, the deformation along the Y direction (vertical direction) due to angular velocity effect (δv) obtained by this analysis is +0.049442 cm (Fig. 11). The positive sign of deformation shows that the crank has been thrown upwards due to centrifugal force. Figure 12 shows the variation of deformation along the length of the crank. The deformation is maximum at the free end of the crank because the centrifugal force is directly proportional to radius of gyration. Similarly, Fig. 13 shows the variation of induced von Mises stress along the length of the crank. The stress is maximum at the shaft end (fixed support end). The maximum value of induced von Mises stress is found to be 1,771 N/cm^2. The total deformation due to inertia and temperature effect δ is obtained from Eq. 8 and the same is listed in Table 6. The relationship between total deformation δ and temperature is determined from deformation vs temperature plot (Fig. 14). The relationship is given by Eq. 9.

Table 5 Mass properties of components crank shaft sub assembly

Sample no	Mass property	Value
1	Volume in mm^3	1.493E+06
2	Mass in kg	11.707
3	IXX about C.G in kg m^2	4.462E+05
4	IYY about C.G in kg m2	1.660E+06
5	IZZ about C.G in kg m^2	2.102E+06
6	Principal M.I-I1 in kg m^2	1.417E+05
7	Principal M.I-I2 in kg m^2	1.965E+06
8	Principal M.I-I3 in kg m^2	2.102E+06
9	Radius of gyration—R1 in mm	110.016
10	Radius of gyration—R2 in mm	409.658
11	Radius of gyration—R3 in mm	423.734

$$\delta = \delta_g + \delta_v = -0.2525 + 0.049442 = -0.20305\,\text{cm} \tag{8}$$

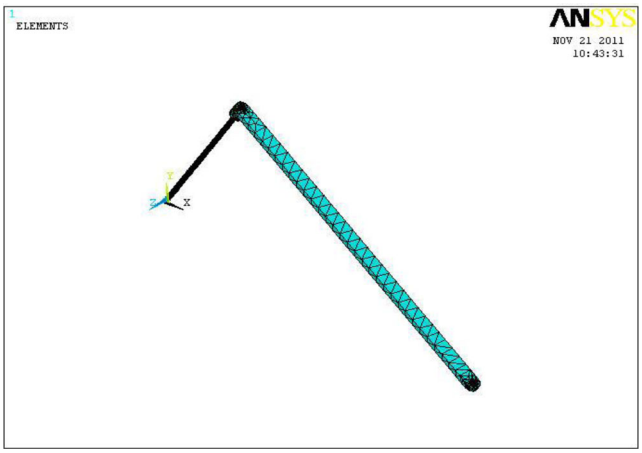

Fig. 10 Finite element model of the crank and shaft subassembly

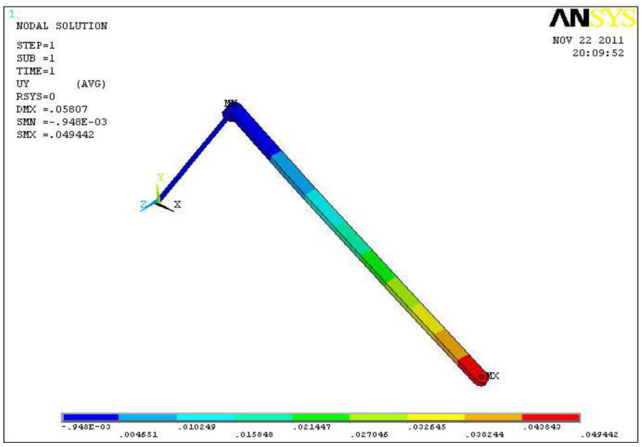

Fig. 11 Deformation along Y direction due to angular velocity effect at 25 °C

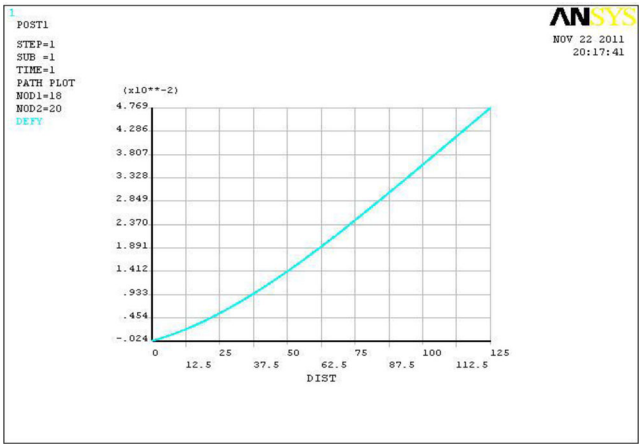

Fig. 12 Deformation-Y plot due to angular velocity effect at 25 °C

$$\delta = (0.0007)\text{Temp} + (0.1863) \tag{9}$$

4 Tolerance design

The tolerance allocation of the motor assembly is carried out as follows. The response variable is total cost [28, 29] which is the sum of manufacturing cost and quality losses and it is expressed as:

$$\text{TC}_i = \sum_{j=1}^{q} k_j \left[\left(U_{ij} - T_j \right)^2 + \sigma_{ij}^2 \right] + \sum_{k=1}^{m} C_M(t_{ik}), \tag{10}$$

where m is the total number of components from q assembly dimensions in a finished product, k_j the cost coefficient of the jth resultant dimension for quadratic loss function, U_{ij} the jth resultant dimension from the ith experimental results, σ_{ij} the

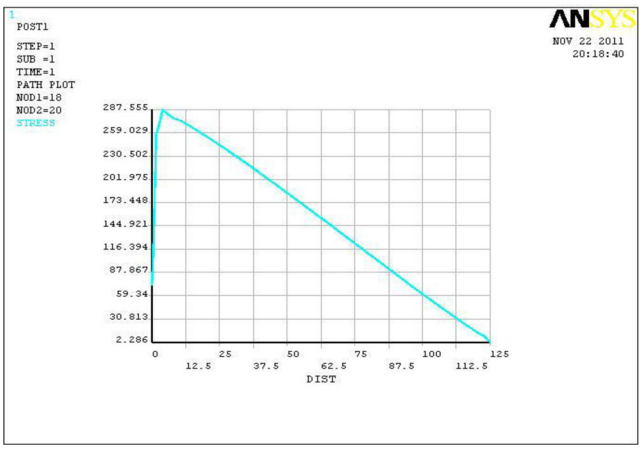

Fig. 13 von Mises stress plot due to angular velocity effect at 25 °C

Table 6 Total deformation for various temperatures

S.No	Temperature (°C)	Deformation (cm)
1	10 °C	0.19301
2	25 °C	0.20305
3	40 °C	0.21311

jth resultant variance of statistical data from the ith experimental results, T_j the design nominal value for the jth assembly dimension, t_{ik} the tolerance established in the ith experiment for the kth component, and CM(t_{ik}) the manufacturing cost for the tolerance t_{ik}.

The variables are x_1 (motor shaft size), x_2 (motor shaft perpendicularity), x_3 (x-base) and x_4 (motor base flatness). Table 7 shows the range of tolerance and respective cost for each variable. The constraint equation for stack up tolerance is obtained by performing sensitivity analysis on the developed computer-aided design (CAD) model. Based on the sensitivity analysis, the clearance is found to be a function of the following feature tolerance. They are x-base flatness, motor base flatness, motor shaft size, and motor shaft perpendicularity.

$$F(x) = (x_1, x_2, x_3, x_4) \leq 0.89 \text{ cm} \tag{11}$$

The value of clearance for any combination of x_1, x_2, x_3, and x_4 values can be retrieved from the CAD model. Table 8 shows the different values of cost for a set of 27 variables. Then neural network model of cost–tolerance function is developed as follows. A Back Propagation (BP) network which has been widely applied to fit the cost–tolerance relationship [11] has been used. The procedure for developing the model is as follows. First, two thirds of experimental results drawn randomly from Table 8 are used to train the neural network. Before applying the neural network for modeling, the architecture of the network has been decided; i.e. the number of hidden layers and the number of neurons in each

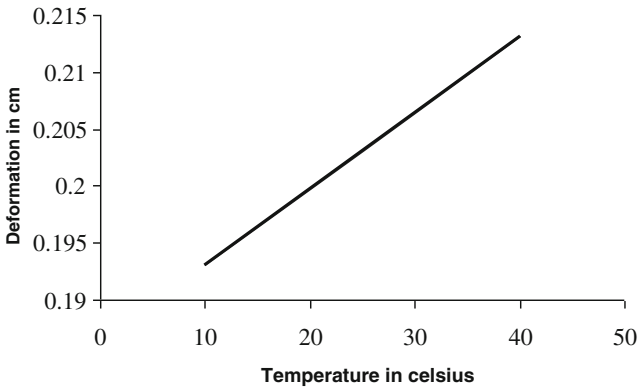

Fig. 14 Deformation vs temperature

Table 7 Tolerance costs for each factor at various levels

Variable	Lower limit	Cost $	Upper limit	Cost $
x1	0.1	18.07	0.2	12.82
*x*2	0.05	35.18	0.1	21.90
x3	0.05	279.61	0.1	108.57
x4	0.04	29.87	0.08	17.98

layer. As there are four inputs and one output, the numbers of neurons in the input and output layer have to be set to 4 and 1 respectively. Also, the BP architecture with one hidden layer is enough for majority of the applications. Hence, only one hidden layer has been adopted. The optimum value of learning rate and momentum coefficient for a network is determined as follows. Initially the momentum coefficient is kept constant and training is carried out for

Table 8 Cost–tolerance relation

Experiment number	*x*-base flatness (x_1)	Motor base flatness (x_2)	Motor shaft size (x_3)	Motor shaft perpendicularity (x_4)	Total cost in $ TC(X)
1	0.15	0.075	0.1	0.08	228.9
2	0.15	0.075	0.1	0.04	239.5
3	0.15	0.075	0.05	0.08	361.3
4	0.15	0.075	0.05	0.04	373.0
5	0.15	0.1	0.075	0.08	266.1
6	0.15	0.1	0.075	0.04	277.6
7	0.15	0.05	0.075	0.08	277.2
8	0.15	0.05	0.075	0.04	289.0
9	0.15	0.1	0.1	0.06	228.4
10	0.15	0.1	0.05	0.06	361.1
11	0.15	0.05	0.1	0.06	240.8
12	0.15	0.05	0.05	0.06	372.5
13	0.2	0.075	0.075	0.08	274.6
14	0.2	0.075	0.075	0.04	286.3
15	0.1	0.075	0.075	0.08	267.0
16	0.1	0.075	0.075	0.04	278.7
17	0.2	0.075	0.1	0.06	236.3
18	0.2	0.075	0.05	0.06	369.9
19	0.1	0.075	0.1	0.06	228.6
20	0.1	0.075	0.05	0.06	362.0
21	0.2	0.1	0.075	0.06	274.6
22	0.2	0.05	0.075	0.06	290.9
23	0.1	0.1	0.075	0.06	266.7
24	0.1	0.05	0.075	0.06	278.3
25	0.15	0.075	0.075	0.06	271.2
26	0.15	0.075	0.075	0.06	268.4
27	0.15	0.075	0.075	0.06	269.9

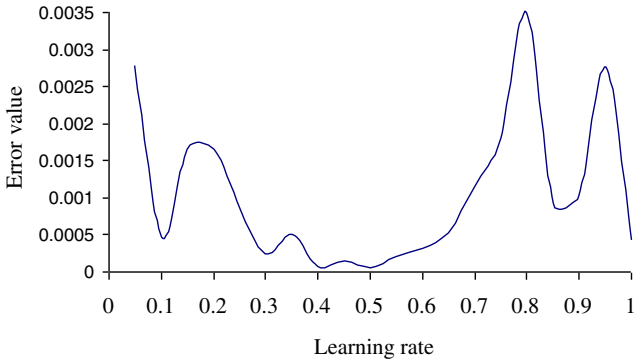

Fig. 15 Error value vs learning rate plot

different values of learning rate say 0.5, 1, 1.5 and so on. Once the optimum value of learning rate is determined based on error value, the optimum value of momentum coefficient is determined by training the network with different values of momentum coefficient. Figures 15 and 16 gives error value vs learning rate plot and error value vs momentum coefficient plot for 4-7-1 architecture.

A procedure was employed to determine the optimum number of neurons in the hidden layer. Accordingly, an experimental approach was adopted, which involved testing the trained neural networks against the remaining one third of experimental results. Experimental and predicted outputs for different number of neurons have been compared.

The regression statistics for different architectures are determined and listed in Table 9 and the same have been plotted against the number of neurons as shown in Fig. 17.

It is observed that the regression statistics were minimized with 7 neurons. Hence, 4-7-1 is the most suitable network for the task under consideration. The training function used in this research is gradient descent with momentum back propagation. The transfer function used in this research is tan-sigmoid and gradient descent weight/momentum weight/bias learning function has been used.

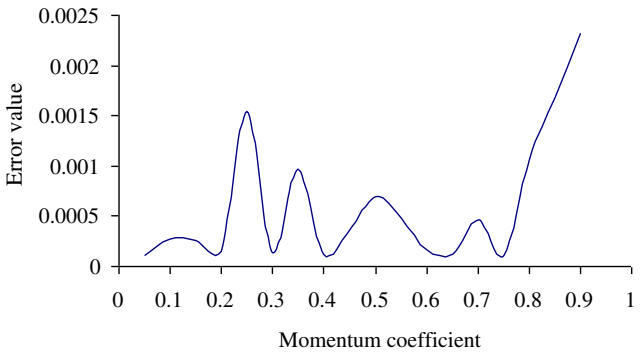

Fig. 16 Error value vs momentum coefficient plot

Table 9 Regression statistics for each network architecture

Network architecture	Mean prediction error %	R square value	Standard error
4-4-1	4.498492501	0.943112	12.06117
4-5-1	2.035675506	0.987509	6.426893
4-6-1	4.100965211	0.902752	16.94439
4-7-1	1.735294596	0.989658	5.608395
4-8-1	3.495912167	0.96686	10.32931
4-9-1	5.935647182	0.725488	33.33576
4-10-1	4.749441739	0.850217	22.10918

Figure 18 shows the schematic diagram of the neural network.

The learning rate=0.4, momentum=0.2 and training epochs=2000. The weights (and biases) are randomly initialized between −0.5 and 0.5. Figure 19 shows the performance of 4-7-1 architecture training.

Once the neural network gets trained, it can provide the result for any arbitrary value of input data set. Table 10 shows the experimental result and the model prediction. It is observed that the prediction based on an artificial neural network (ANN) model is quite close to the experimental observation.

The neural network model for the above problem is developed as per the approach discussed previously. Based on those discussions, the BP network of 4-7-1 architecture produces the best performance (refer to Table 11) and the same is adopted to generate the neural network based cost–tolerance function under this case study. Comparison of experimental results with artificial neural network model prediction for other architecture is shown in Table 12.

The optimization problem is solved by nondominated sorting genetic algorithm II optimization algorithm (NSGA II). The solution of the motor assembly case can be found by solving the following mathematical models.

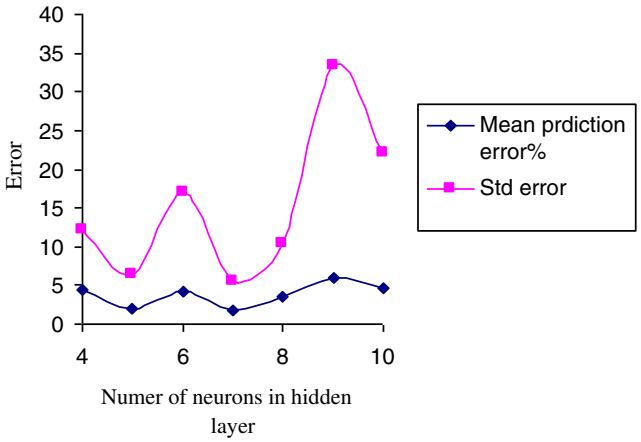

Fig. 17 Error versus the number of neurons in a hidden layer

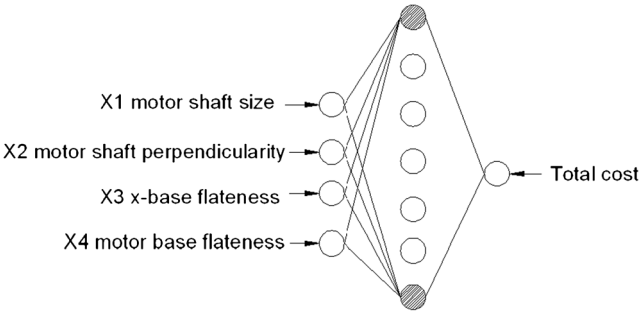

Fig. 18 Schematic diagram of the neural network

$$\left\{\begin{array}{l}\text{Maximize TC}_i = \sum_{j=1}^{q} k_j\left[\left(U_{ij}-T_j\right)^2+\sigma_{ij}^2\right]+\sum_{k=1}^{m} C_M(t_{ik})\\ \text{subject to}\\ \text{clearance } F(x)=(x_1,x_2,x_3,x_4)\le 0.89\,\text{cm}\\ 0.1\le x_1\le 0.2,\\ 0.05\le x_2\le 0.1,\\ 0.05\le x_3\le 0.1,\\ 0.04\le x_4\le 0.08.\end{array}\right. \tag{12}$$

The outline of the proposed optimization strategy is shown in Fig. 20. Once a set of tolerance corresponding to minimum cost has been determined by NSGA II, the tolerance values are fed in to the interactive CAD model in order to determine the clearance value. The results of FEA show that the various components of the assembly undergo deformation due to the inertia effect, thereby reducing the clearance by 0.20305 cm. The reduction in clearance caused by the deformation is independent of tolerance values. So the deformation can be included in the constraint equation (Eq. 13), which in turn

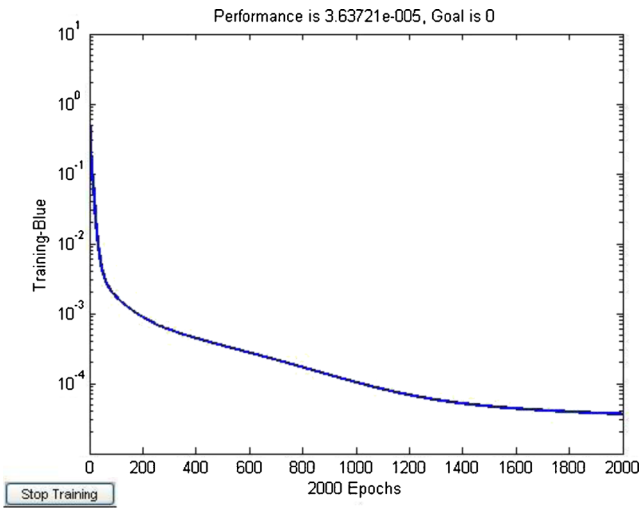

Fig. 19 Performance of 4-7-1 architecture

Table 10 Comparison of experimental results with the ANN model prediction

Total cost in $ TC(X) Experimental results	Predicted value by ANN	Prediction error (%)
239.517	233.5125993	2.506878729
373.02	370.1791799	0.761573146
228.449	229.8694101	0.621762439
361.1	353.4342438	2.12289012
266.993	269.1789878	0.818743499
236.277	234.1075089	0.918198157
274.648	270.9355255	1.351720937
266.679	251.1227928	5.833307915
271.192	269.3409074	0.682576422
Maximum prediction error for each output in this row in %		5.833307915
Minimum prediction error for each output in this row in %		0.621762439
Mean prediction error for each output in this row in %		1.735294596

increases the tolerance values, thereby reducing the manufacturing cost. The modified constraint equation for stack up tolerance is given as follows:

$$F(x) = (x_1, x_2, x_3, x_4) \leq 0.89 + \delta \tag{13}$$

where δ is total deformation which is a function of temperature (Eq. 9). The least cost is found to be $ 230.3739. The solution converges in the 38th generation. The NSGA II optimization results for the proposed method are given in Table 12.

Table 11 Comparison of experimental results with the ANN model prediction for 4-7-1 network architecture

Total cost in $ TC(X) Experimental results	Predicted value by ANN	Prediction error (%)
239.517	233.5125993	2.506878729
373.02	370.1791799	0.761573146
228.449	229.8694101	0.621762439
361.1	353.4342438	2.12289012
266.993	269.1789878	0.818743499
236.277	234.1075089	0.918198157
274.648	270.9355255	1.351720937
266.679	251.1227928	5.833307915
271.192	269.3409074	0.682576422
Maximum prediction error for each output in this row in %		5.833307915
Minimum prediction error for each output in this row in %		0.621762439
Mean prediction error for each output in this row in %		1.735294596

Table 12 NSGA II optimization result for proposed method

Gen. no	Min. objec.	Gen. no	Min. objec.
1	383.8660	21	275.8378
2	365.5328	22	269.6216
3	350.3704	23	268.9944
4	345.4331	24	266.7900
5	345.0194	25	266.7900
6	332.4663	26	259.6442
7	328.0760	27	256.3991
8	324.6031	28	253.2321
9	323.9611	29	252.3969
10	321.5415	30	250.2312
11	321.1886	31	248.3452
12	312.0675	32	248.0548
13	309.5702	33	245.8765
14	307.6479	34	240.6544
15	299.1952	35	237.2133
16	299.1520	36	235.1236
17	288.4992	37	231.3478
18	286.0766	38	230.3739
19	283.3560	39–100	230.3739
20	276.3634		

5 Results and discussions

The solution of the motor assembly process was found by solving the mathematical model (Eq. 12) using NSGA II. Initially, the problem is solved for rigid body condition, in which all the components in the assembly are considered as rigid body. The NSGA II specific parameters for the tolerance design problem are listed in Table 13. The optimal values of tolerance and total cost obtained are compared with corresponding values obtained by response surface method [29] (Table 14). The total cost obtained by the NSGA II is found to be less than those values. Due to considerable saving in cost, NSGA II is selected as optimization tool for the proposed methodology. The optimal values of tolerance, manufacturing cost and quality loss determined using NSGA II for rigid body approach are compared with those values obtained for the proposed method (Table 15). By comparing the optimal values, considerable cost savings are obtained for the proposed methodology than the rigid body approach. The reasons for the cost savings are as follows.

In the proposed methodology, BP neural network is used to develop the cost–tolerance model. The neural network model

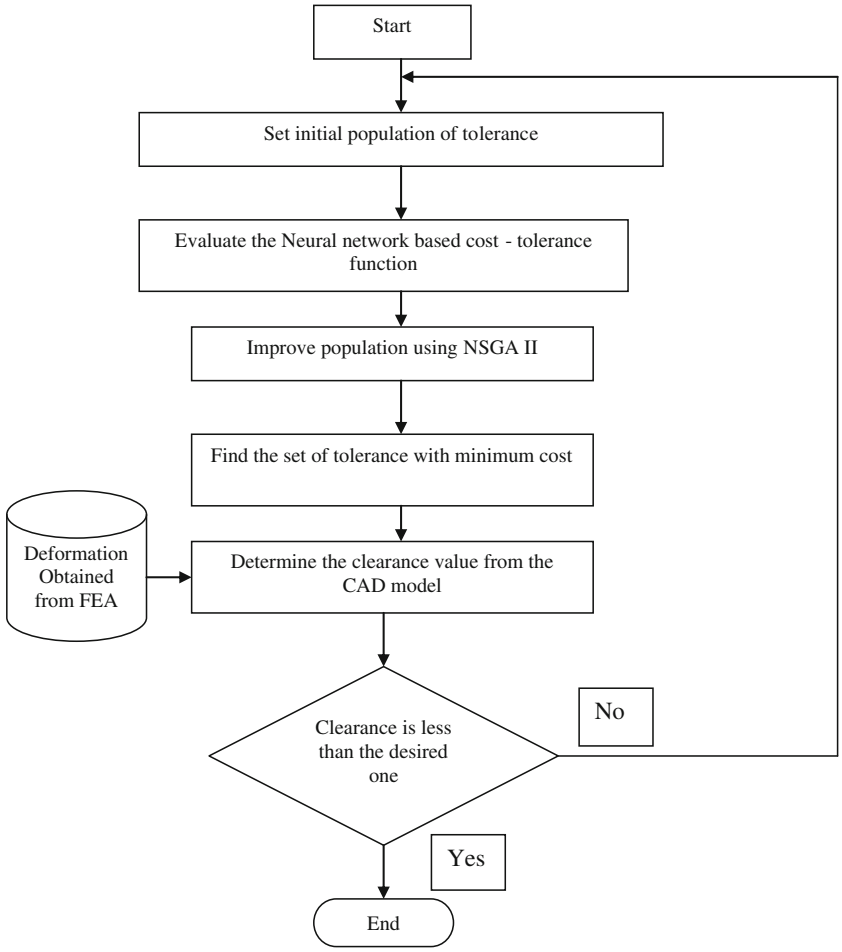

Fig. 20 Proposed optimization strategy

developed is found to have better regression statistics due to less fitting error. Table 10 shows the comparison of experimental results with the artificial neural network model prediction, where mean prediction error for each output is found to be 1.735 %. The optimization of the above model has yielded better result due to less fitting error.

In the proposed methodology, all the components are considered as deformable bodies and the deformations are determined by FEA. The predetermined values of deformation are suitably incorporated in the constraint equation of the tolerance design problem. Due to this, the tolerance requirements of the given assembly are relaxed to certain extent for critical components, resulting in reduced manufacturing cost.

The optimal tolerance values obtained for the proposed methodology are higher than those obtained by the rigid body approach. This results in higher quality loss than that of the rigid body approach. The increase in the quality loss is much less compared to the decrease in the manufacturing cost. Thus, the total cost, which is the sum of manufacturing cost and quality loss cost, is less than that of the rigid body approach.

Table 13 NSGA II specific data

Parameter	Value
Variable type	Real variable
Population size	100
Cross over type	Binomial
No of difference vector	1
Vector to be perturbed	Random
Total no of generation	100
No of variables	4

Table 14 Comparison of optimal value of tolerance and total cost

Sample no	Variable	Optimal value of tolerances in cm		Total cost in $		% Cost savings
		RSM	NSGA II	RSM	NSGA II	
1	x_1	0.14181	0.1	238.5191	232.1907	2.65 %
2	x_2	0.080894	0.081125			
3	x_3	0.098334	0.1			
4	x_4	0.064308	0.07799			

Table 15 Comparison values of optimal obtained by rigid body approach and the proposed method for operating temperature 25 °C

Method	Parameter	Rigid body approach	The proposed method	% Cost savings
Parametric CAD model	x_1	0.1	0.086439	12.77 %
	x_2	0.081125	0.08	
	x_3	0.1	0.106116	
	x_4	0.07799	0.078027	
	Manufacturing cost	$ 189.478	$ 191.354	
	Quality loss	$ 42.713	$ 39.019	
	Quality loss due to deformation	Nil	Nil	
	Total cost	$ 264.089	$ 230.3739	

In the rigid body approach, an additional quality loss is generated due to actual deformation of the components. When the components are assembled into a product, some of the flexible components like shaft, bearing, etc., in this application problem, are more flexible than the other components and they undergo significant deformation due to thermal and gravity effects. In the proposed methodology, there is no additional quality loss due to deformation as the deformations are included in the constraint equations of the tolerance design problem.

Due to the above reasons, the proposed methodology is found to produce assemblies of less cost than that of the rigid body approach.

Similarly, the optimal values of tolerance can be obtained for operating temperature 10 and 40 °C. In case of 10 °C, the operating temperature being 15 °C less than the room temperature results in contraction of length of gear shaft compared to its length at room temperature. This in return reduces the value of δ, thereby tightening the tolerance requirement than that of the room temperature, which results in increase of total manufacturing cost. In case of 40 °C, the gear shaft expand to a length more than the room temperature, thereby loosening the tolerance requirement resulting in decrease of total manufacturing cost. Table 16 shows the optimal values of tolerances obtained for operating temperature 10 and 40 °C.

Table 16 Optimal values of tolerances obtained by the proposed method for operating temperature 10 °C and 40 °C

Method	Parameter	Optimal values	
Parametric CAD model		10 °C	40 °C
	x_1	0.080538	0.090650
	x_2	0.08	0.08
	x_3	0.106010	0.107226
	x_4	0.070025	0.079927
	Manufacturing cost	$ 199.017	$ 188.933
	Quality loss	$ 36.520	$ 36.520
	Quality loss due to deformation	Nil	Nil
	Total Cost	$ 235.537	$ 225.453

6 Conclusion

In this work, an integrated tolerance design approach was adopted where the effect of deformation of all parts of the assembly due to inertia and change in operating temperature has been considered. A parametric CAD model of the assembly has been developed by including dimensional and geometric tolerances in addition to effect of geometric tolerance on various kinematic joints of the assembly (Figs. 4 and 5). Then, sensitivity analysis is carried out on the model to determine critical features of the assembly. The deformation of the assembly model is determined using FEA. The deformation of the assembly due to inertia effect has been determined (Fig. 7). The deformation of rotating parts of the sub assembly due to angular velocity and change in temperature has also been determined (Fig. 11). The values of total deformation have been determined for different operating temperature (Table 6). The total deformation is found to have a linear relationship with operating temperature (Eq. 9). Due to this deformation, the critical assembly feature is reduced. So, the tolerance of the critical assembly feature has been increased. Instead of regression model, artificial neural network model has been used to develop cost–tolerance relationship thereby reducing fitting error. Optimization of tolerance design has been carried out where the value of critical assembly feature has been retrieved from the CAD model. By this method, the total manufacturing cost has been reduced by 12.77 %. Significant reduction of total manufacturing cost has been obtained using this methodology. This methodology can be adopted for development of a customized software program which paves the way for futuristic tolerance design of mechanical assemblies in industries.

References

1. Zhang C, Wang B (1993) The discrete tolerance optimization problem. Manuf Rev 6(1):60–71
2. Al-Ansary MD, Deiab IM (1997) Concurrent optimization of design and machining tolerances using the genetic algorithms method. Int J Mach Tools Manuf 37(12):1721–1731
3. Chase KW, Greenwood WH, Loosli BG, Haugland LH (1999) Least cost tolerance allocation of mechanical assemblies with automated process selection. Manuf Rev 3(1):49–59

4. Dong Z, Hu W, Xue D (1994) New production cost–tolerance models for tolerance synthesis. ASME Trans J Eng Ind 116:199–206
5. Lee WJ, Woo TC (1989) Optimum selection of discrete tolerances. Trans ASME J Mech Trans Auto Des 111:243–252
6. Lee WJ, Woo TC, Chou SY (1993) Tolerance synthesis for non linear systems based on nonlinear programming. IIE Trans 25(1): 51–61
7. Taguchi G (1989) Quality engineering in production systems. McGraw-Hill, New York
8. Chen RM, Chan WW (1993) Efficient tolerance design procedure for yield maximization using optimization techniques and neural network, in Proc. IEEE Int. symposiums on circuits and systems
9. Kopardekar P, Anand S (1995) Tolerance allocation using neural networks. Int J Adv Manuf Technol 10:269–276
10. Stern HS (1996) Neural networks in applied statistics. Technometrics 38:205–220
11. Chen MC (2001) Tolerance synthesis by neural learning and nonlinear programming. Int J Prod Econ 70:55–65
12. Lin ZC, Chang DY (2002) Cost-tolerance analysis model based on neural network method. Int J Prod Econ 40(6):1429–1452
13. Yang CC, Achutha Naikan VN (2003) Optimum design of component tolerances of assemblies using constraint networks. Int J Prod Econ 84:149–163
14. Liu SC, Hu SJ (1997) Variation simulation for deformable sheet metal assembly using finite element methods. Trans ASME J Manuf Sci Eng 119:368–374
15. Camelio JA, Hu SJ, Ceglarek DJ (2001) Modeling variation propagation of multi-station assembly systems with compliant parts, in Proc. DETC'01 ASME
16. Hu SJ (1997) Stream-of-variation theory for automotive body assembly. Annals CIRP 46(1):1–6
17. Ceglarek DJ, Shi J (1997) Tolerance analysis for sheet metal assembly using a beam-based model. ASME, Int Mech Engg Cong Expos, DE, 94:153–159
18. Hu M, Lin ZQ, Lai XM, Ni J (2001) Simulation and analysis of assembly process considering compliant, non-ideal parts and tooling variations. Int J Mach Tools Manuf 41:2233–2243
19. Hsieh CC, Oh KP (1997) A framework for modeling variation in vehicle assembly processes. Int J Veh Des 18(5):466–473
20. Sampers S, Giordano M (1998) Taking into account displacements in 3D tolerancing models and application. J Mater Process Technol 78 (1):156–167
21. Liao X, Wang GG (2005) Employing fractals and FEM for detailed variation analysis of non rigid assemblies. Int J Mach Tools Manuf 45:445–454
22. Manarvi IA, Juster NP (2004) Framework of an integrated tolerance synthesis model and using FE simulation as a virtual tool for tolerance allocation in assembly design. J Mater Process Technol 150:182–193
23. Pierre L, Teissandier D, Nadeau JP (2009) Integration of thermo-mechanical strains into tolerance analysis. Int J Adv Manuf Technol 3 (4):247–263
24. Jayaprakash G, Sivakumar K, Thilak M (2012) Tolerance design of mechanical assembly using NSGA II and finite element analysis. J Mech Sci Technol 26(10):3261–3268
25. Jayaprakash G, Sivakumar K, Thilak M (2012) A numerical study on effect of temperature and inertia on tolerance design of mechanical assembly. Eng Comput 29(7):722–742
26. Shen Z, Ameta G, Shah JJ, Davidson J, Davidson JK (2005) A comparative study of tolerance analysis methods. ASME J Comput Inf Sci Eng 5:247–256
27. Gao J, Chase KW, Magleby SP (1998) General 3-D tolerance analysis of mechanical assemblies with small kinematic adjustments. IIE Trans 30:367–377
28. Jeang A (1995) Economic tolerance design for quality. Qual Reliab Eng Int 11(2):113–121
29. Jeang A, Lieu E (1999) Robust tolerance design by computer experiment. Int J Prod Res 37(9):1949–1961